Ultraslow settling kinetics of frictional cohesive powders

Kai Nan and Robert S. Hoy*

Department of Physics, University of South Florida, Tampa, FL 33620
(Dated: December 12, 2022)

Using discrete element method simulations, we show that the settling of frictional cohesive grains under ramped-pressure compression exhibits strong history dependence and slow dynamics that are not present for grains that lack either cohesion or friction. Systems prepared by beginning with a dilute state and then ramping the pressure to a small positive value $P_{\rm final}$ over a time $\tau_{\rm ramp}$ settle at packing fractions given by an inverse-logarithmic rate law, $\phi_{\rm settled}(\tau_{\rm ramp}) = \phi_{\rm settled}(\infty) + A/[1 + B\ln(1 + \tau_{\rm ramp}/\tau_{\rm slow})]$. This law is analogous to the one obtained from classical tapping experiments on noncohesive grains, but crucially different in that $\tau_{\rm slow}$ is set by the slow dynamics of structural void stabilization rather than the faster dynamics of bulk densification. We formulate a kinetic free-void-volume theory that predicts this $\phi_{\rm settled}(\tau_{\rm ramp})$, with $\phi_{\rm settled}(\infty) = \phi_{\rm ALP}$ and $A = \phi_{\rm settled}(0) - \phi_{\rm ALP}$, where $\phi_{\rm ALP} \equiv .135$ is the "adhesive loose packing" fraction found by Liu *et al.* [W. Liu, Y. Jin, S. Chen, H. A. Makse and S. Li, *Soft Matt.* **13**, 421 (2017)].

The structure of granular solids is famously preparation-protocol-dependent. For example, mechanical excitation by periodic tapping makes samples' packing fractions increase logarithmically in time:

$$\phi(t) = \phi(\infty) - \frac{A}{1 + B\ln(1 + t/\tau_{\rm slow})}, \qquad (1)$$

where A, B, and $\tau_{\rm slow}$ depend on the sample-preparation and tapping protocols in addition to the intergrain interactions [1, 2]. This density increase is directly analogous to, but typically far greater in extent than, the density increase experienced by aging thermal glasses [3]; both arise from the slow, activated dynamics of systems traversing the rugged energy landscapes that are a common feature of thermal glasses and granular materials [4, 5]. Cohesive interactions greatly slow the dynamics of viscous liquids [6], and frictional interactions greatly slow the dynamics of granular solids [7, 8]. One might expect that the combination of frictional and cohesive interactions will produce a further dynamical slowdown, and indeed it does. In particular, the combination of cohesive interactions, rolling, sliding, and twisting friction can arrest compaction entirely – at least on human time scales – by mechanically stabilizing large "structural" voids within marginally jammed packings [9–14].

As a consequence, unlike their frictionless or purely-repulsive counterparts, frictional cohesive granular solids can be prepared with a very wide range of densities. For example, the Hausner ratio $H = \rho_{\rm tapped}/\rho_{\rm settled}$ [15], where $\rho_{\rm settled}$ is the density obtained by pouring grains into a container and $\rho_{\rm tapped}$ is the density obtained in the long-time limit of a tapping experiment, is a commonly employed measure of powder flowability. H is also a measure of the range of jamming densities ϕ_J obtainable via different preparation protocols, i.e. different protocols will produce $\phi_{\rm min} \leq \phi_J \leq \phi_{\rm max} \equiv H\phi_{\rm min}$. H has long been known to increase with decreasing particle size, approaching 4 for micron-size grains, because smaller grains are more cohesive than their larger counterparts [16, 17]. More recently it has been explicitly shown that H values for fixed-size grains increase rapidly with both cohesion and friction [11, 18], and recent simulations that established an equation of state for random sphere packings [19, 20] suggest that spherical grains' $H \to H_{\rm max} \simeq 3.8$ in the limit of strong cohesion and friction.

Using H as a measure of powder flowability is often criticized on the grounds that both $\rho_{\rm tapped}$ and $\rho_{\rm settled}$ are preparation-protocol dependent [21]; in general, reproducible values of H are obtained only when highly specific standardized procedures are followed [22]. The interplay of cohesion and friction in determining the history-dependence of both "static" macroscopic quantities like $\rho_{\rm settled}$ and microscopic (grain-level) structure in these powders remains poorly understood and the subject of active study [23–25]. In particular, while the logarithmically slow densification of noncohesive and frictionless cohesive granular materials has been semiquantitatively explained by kinetic free-volume theories [26–29], microscopic-physics-based theories that accurately predict the preparation-protocol-dependent $\phi(t)$ [including $\phi(0) \equiv \phi_{\rm settled}$] for frictional cohesive powders have yet to be developed, and doing so is very challenging owing to additional complications associated with the abovementioned mechanically stable structural voids. Developing such theories could prove useful for applications ranging from avalanche prevention [30] to pharmaceuticals [31] to additive manufacturing [32].

In this Letter, we use discrete element method (DEM) simulations to examine how the structure of marginally jammed systems of grains with varying degrees of friction and cohesion depends on the compression protocol used to prepare them. We compare results for model systems with four types of intergrain interactions: (1) no friction or cohesion, (2) all three types of friction (sliding, rolling, and twisting) but no cohesion, (3) cohesion but no friction, and (4) both cohesion and friction. The settled packing fractions of systems prepared by beginning with a dilute state and then linearly ramping the pressure to a fixed, small value $P_{\rm targ}$ over a time $\tau_{\rm ramp}$ decrease as co-

* rshoy@usf.edu

hesion and friction are increased, ranging from the canonical random-close-packed value ($\phi_{\mathrm{RCP}} = 0.646$ [33, 34]) for model 1 to as low as 0.35 for model 4. While these ϕ_{settled} are almost independent of τ_{ramp} for models 1-3, they decrease substantially with increasing τ_{ramp} for model 4, reaching their asymptotic low-rate limit at a τ_{ramp} that is many orders of magnitude larger than the corresponding values for models 1-3.

This behavior is the opposite of the usual glass-jamming paradigm [4, 35], in which thermal glasses and granular materials end up with higher densities when they are more slowly cooled or compressed. We find that the rate-dependence of model 4's ϕ_{settled} is described by

$$\phi_{\mathrm{settled}}(\tau_{\mathrm{ramp}}) = \phi_{\mathrm{settled}}(\infty) + \frac{A}{1 + B\ln\left(1 + \tau_{\mathrm{ramp}}/\tau_{\mathrm{slow}}\right)}, \tag{2}$$

and argue that the difference leading to the crucial change in sign (from $-$ to $+$) is that while the τ_{slow} in Eq. 1 is set by the slow dynamics of densification [1, 2], the τ_{slow} in Eq. 2 is set by the even slower dynamics of *structural void stabilization*. Then we formulate a kinetic free-void-volume theory (similar in spirit to but different in several crucial details from those of Refs. [26–29]) that predicts this behavior, with $\phi_{\mathrm{settled}}(\infty) = \phi_{\mathrm{ALP}}$ and $A = \phi_{\mathrm{settled}}(0) - \phi_{\mathrm{ALP}}$, where $\phi_{\mathrm{ALP}} \equiv .135$ is the "adhesive loose packing" fraction found by Liu *et al.* [19, 20].

Our simulations aim to implement realistic viscoelastic, cohesive and frictional interactions in a way that is computationally cheap enough to allow us to simulate large systems over long timescales. Therefore we choose to employ the Hertzian variant of the widely-used Rognon potential [36, 37] for the conservative pair interactions. A standard radial damping force [38] is added to capture viscous dissipation. Sliding friction is implemented using the widely used linear-history model [39], while rolling and twisting friction are implemented using the same methods as Santos *et al.* [40, 41]. Ref. [40] showed that this combination of intergrain interactions accurately reproduces the packing fractions and coordination numbers found in typical experiments [24, 42–44]. Since we wish to consider the limit of strong friction in this study, we set the sliding, rolling, and twisting friction coefficients to 0.5. All interactions are described in detail in the Supplementary Materials; all quantities discussed below are expressed in dimensionless units.

DEM simulations are performed using LAMMPS [47]. Following Ref. [40], we begin by placing $N = 10^5$ particles randomly within a periodic cubic simulation cell of volume $V = 39N\pi/(125\phi_{\mathrm{init}})$, where $\phi_{\mathrm{init}} = .05$ is the initial packing fraction. Then a slow pushoff is run (at constant ϕ) to eliminate high-energy particle overlaps; the liberated energy is removed by damping the particle velocities until an athermal state is obtained. After the pushoff is completed, "settled" states are prepared using a procedure that mimics pouring a powder into a container at a rate $R_P \sim \tau_{\mathrm{ramp}}^{-1}$, but removes complications associated with pouring experiments' anisotropic "external" forces (i.e. gravity and the container walls).
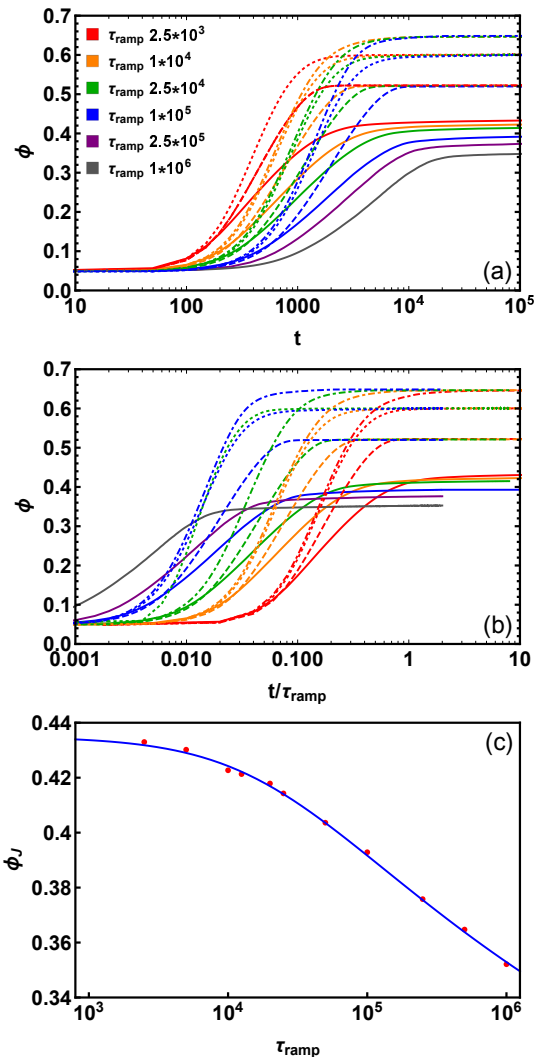

FIG. 1. Influence of intergrain interactions and preparation protocol on powder settling. Panels (a-b) respectively show $\phi(t)$ and $\phi(t/\tau_{\mathrm{ramp}})$ for a wide range of τ_{ramp}. Dot-dashed, dotted, dashed and solid curves respectively show results for models 1-4. All results for models 1-3 are consistent with many previous studies, e.g. Refs. [19, 20, 40, 45, 46]. Panel (c) shows the settled densities $\phi_{\mathrm{settled}} = \phi(10\tau_{\mathrm{ramp}})$ for frictional cohesive grains (model 4). Red symbols show simulation data and the blue curve shows Eq. 2 with $\phi_{\mathrm{settled}}(\infty) = 0.135$, $A = 0.300$, $B = 0.098$, and $\tau_{\mathrm{slow}} = 2.2 \cdot 10^4$.

We ramp the applied hydrostatic pressure from 0 to $P_{\mathrm{targ}} = 10^{-3}$ over a time τ_{ramp} and afterwards hold it constant for least another 10^5 time units. In other words, the applied stresses along the x, y and z directions are $\sigma_{xx} = \sigma_{yy} = \sigma_{zz} = P_{\mathrm{targ}}t/\tau_{\mathrm{ramp}}$ for $t \leq \tau_{\mathrm{ramp}}$, and $\sigma_{xx} = \sigma_{yy} = \sigma_{zz} = P_{\mathrm{targ}}$ for $t \geq \tau_{\mathrm{ramp}}$ [48, 49]. Since $P_{\mathrm{targ}} = 10^{-3}$ is large enough for the employed Nose-Hoover barostat to be effective yet small enough to minimize plastic consolidation [12, 13], we define all systems' ϕ_{settled} as their $\phi(\tau_{\mathrm{ramp}} + 10^5)$. This definition closely corresponds to the ϕ_{settled} that could be measured after the termination of a pouring experiment.

Figure 1 shows the $\tau_{\rm ramp}$-dependent responses for all four models. As expected, results for repulsive frictionless spheres (model 1) show negligible preparation-protocol dependence. All systems settle at $\phi \simeq 0.646$; this density is consistent with random close packing [33, 34]. The $\phi(t)$ curves nearly collapse when replotted vs. $t/\tau_{\rm ramp}$, at least for $t/\tau_{\rm ramp} > 1$ [panel (b)]. For smaller $t/\tau_{\rm ramp}$, ϕ increases with increasing $\tau_{\rm ramp}$ owing to well-understood kinetic effects associated with the hard sphere glass transition [50]. Comparable preparation-protocol independence of the final jammed states and collapse of the $\phi(t)$ curves occurs for systems with friction but no cohesion (model 2) or cohesion but no friction (model 3), but at lower $\phi_{\rm settled}$. Model 2 systems have $\phi_{\rm settled} \simeq 0.60$, which is consistent with the results of Santos *et al.* [40] for our employed value of $P_{\rm targ}$. Model-3 systems have $\phi_{\rm settled} \simeq 0.52$, which is consistent with adhesive close packing [19, 20] in the presence of the finite-range attractive intergrain interactions (which favor finite particle overlap) employed in this study. These models do not show any evidence of compaction dynamics that are significantly slower than those of model 1. Indeed their $\phi(t)$ actually converge slightly faster, perhaps because their $\phi_{\rm settled}$ are lower and hence their nearly-settled states have more free volume.

Results for systems with both cohesion and friction (model 4) are radically different. Their $\phi(t/\tau_{\rm ramp})$ increase (decrease) monotonically with increasing $\tau_{\rm ramp}$ for $t/\tau_{\rm ramp} \ll 1$ ($t/\tau_{\rm ramp} \gtrsim 1$), and are still increasing logarithmically slowly at $t = 10\tau_{\rm ramp}$ in a manner reminiscent of tapping experiments [1, 2], but show no evidence of convergence towards history-independent values. As shown in panel (c), our results can be well fit by Eq. 2. We assumed $\phi_{\rm settled}(\infty) = \phi_{\rm ALP}$ since this is the packing fraction expected in the limit of large system size and slow compression for systems with very strong cohesion and friction [20]. $A \simeq 0.300$ is a fitting parameter capturing the range of ϕ obtainable as pressure ramping varies from infinitely fast to infinitely slow. $B \simeq 0.098$ is a fitting parameter capturing the relative importance of the logarithmic term [29]. Finally, $\tau_{\rm slow} \simeq 2.2 \cdot 10^4$ is a time scale capturing model 4's inherently slow dynamics.

Clearly Eq. 2 is directly analogous to Eq. 1, but with a crucial difference. Longer tapping duration produces higher densities, whereas slower pressure ramping produces *lower* densities. The latter behavior is the opposite of the usual glass-jamming paradigm [4, 35], in which thermal glasses and granular materials end up with higher densities when they are more slowly cooled or compressed. The $-$ sign between the two terms in Eq. 1 is associated with the slow dynamics of densification in tapped systems [1]; comparable dynamics control densification of aging thermal glasses [3]. In contrast, as we will show below, the $+$ sign between the two terms in Eq. 2 is associated with a slow dynamics of *void stabilization*.

We monitored void growth and coalescence by dividing the DE simulation cells into $N_{\rm c}(t) = n_x(t) \times n_y(t) \times n_z(t)$ subcells of side lengths $\ell_x(t) = L_x(t)/{\rm floor}[{\rm L_x}(t)]$, $\ell_y(t) =$
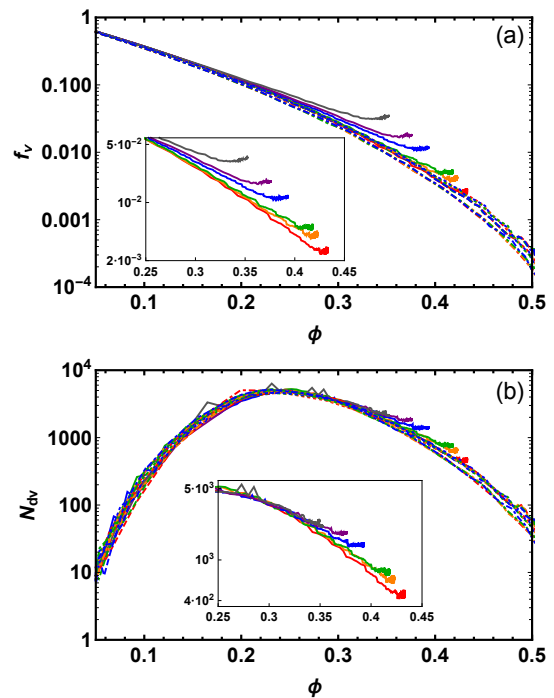

FIG. 2. Void volume fraction $f_{\rm v}$ [panel (a)] and number of topologically distinct voids $N_{\rm dv}$ [panel (b)]. Insets highlight the void stabilization that occurs for model 4. All colors and line types are the same in Fig. 1.

$L_y(t)/{\rm floor}[{\rm L_y}(t)]$, and $\ell_z(t) = L_z(t)/{\rm floor}[{\rm L_z}(t)]$; here floor$[\xi]$ rounds ξ downward to the nearest integer. A subcell is classified as a void if it intersects no (i.e., contains no portion of any) particle cores, where the core of particle j is the sphere of radius R_j centered at $\vec{r}_j$. Thus void subcells are subcells inside which at least one small particle can be placed without contacting any other particles. The void volume fraction is defined as $f_{\rm v}(t) = N_{\rm vc}(t)/N_{\rm c}(t)$, where $N_{\rm vc}(t)$ is the total number of void subcells. We divide these $N_{\rm vc}(t)$ void subcells into $N_{\rm dv}(t)$ distinct (topologically disconnected) voids using connected-components analysis [51], and define structural voids as distinct voids of volume ≥ 10.

Results for all systems are shown in Figure 2. For models 1-3, $f_{\rm v}$ decreases approximately exponentially with ϕ and drops to zero (to within our statistical accuracy) by $\phi \simeq 0.55$. Cohesive systems have larger $f_{\rm v}$ than their noncohesive counterparts for all ϕ, largely because their constituent grains are more likely to form compact clusters at lower ϕ [52–54], but the slopes $d[\ln(f_{\rm v})]/d\phi$ are similar for all three models. As compression continues, $-d[\ln(f_{\rm v})]/d\phi$ increases as void-filling becomes more coherent, i.e. as free volume decreases and particles are increasingly likely to get pushed into empty regions by their interactions with other particles. Results for $N_{\rm dv}(\phi)$ show complementary trends. As compression proceeds, $N_{\rm dv}$ initially increases as large voids are split into smaller ones (recall that a homogeneous system in the low-ϕ limit would have $N_{\rm dv} = 1$), then decreases as these small voids

get filled. For $\phi \gtrsim 0.4$, most voids consist of only one or two subcells, so N_{dv} roughly tracks f_{v}.

Model 4 systems' void statistics follow similar trends at low ϕ. Their $f_{\mathrm{v}}(\phi)$ are slightly higher than their model-3 counterparts, presumably because the compact clusters they form are mechanically stabilized by their frictional interactions and hence are more likely to grow as compression continues [55]. As compression continues, however, the behavior of these systems again becomes qualitatively different from that of models 1-3. Both $f_{\mathrm{v}}(\phi)$ and $N_{\mathrm{dv}}(\phi)$ begin rising substantially above the common exponential trends, at packing fractions ϕ_{vso} that decrease rapidly with increasing τ_{ramp}. Evidently these $\phi_{\mathrm{vso}}(\tau_{\mathrm{ramp}})$ correspond to the onset of structural voids' mechanical stabilization, with lower ϕ_{vso} leading to larger final f_{v} and N_{dv} and therefore also to lower ϕ_{settled}.
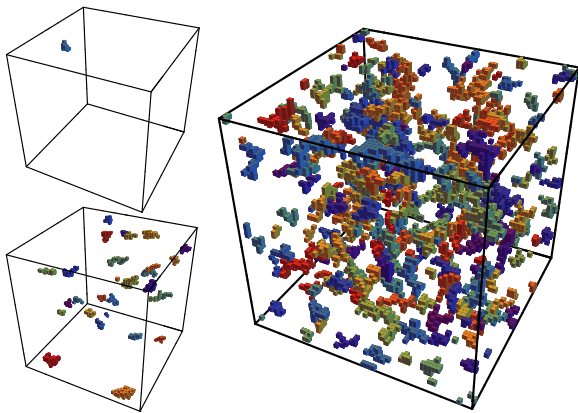

FIG. 3. Structural voids in model 4's final settled states. The upper left, lower left, and right images respectively show results for $\tau_{\mathrm{ramp}} = 10^4$, 10^5 and 10^6; different colors indicate topologically distinct voids.

Visualizing these voids both illustrates the above arguments and reveals a feature that was not apparent from the f_{v} and N_{dv} data alone. Figure 3 shows how increasing τ_{ramp} *qualitatively* alters the final structural-void geometry. For $\tau_{\mathrm{ramp}} = 10^4$, only one small structural void (of volume 11) is present in the settled configuration. In contrast, the settled configurations for $\tau_{\mathrm{ramp}} = 10^5$ ($\tau_{\mathrm{ramp}} = 10^6$) contain 27 (218) structural voids, with volumes as large as 48 (261). Thus larger τ_{ramp} lead not only to larger f_{v} and correspondingly lower ϕ_{settled}, but also to dramatic increases in the number and maximum size of structural voids, and consequently in the settled states' spatial heterogeneity. Note that the final settled states for models 1-3 have *no* structural voids for the range of τ_{ramp} considered here, and their large-scale spatial heterogeneity [as indicated, e.g., by the low-q limit of the static structure factor $S(q)$] is τ_{ramp}-independent.

The first theories that successfully explained the logarithmically slow increase of $\phi(t)$ during tapping experiments (Eq. 1) did so by noting that free volume decreases exponentially, and therefore the characteristic time between relaxation events that lead to further densifica-

tion increases exponentially, with increasing ϕ [26–28]. In the same spirit, we postulate that the kinetic effects of increasing the void volume fraction $\phi_v \equiv 1 - \phi$ towards $1 - \phi_{\mathrm{ALP}}$ in a settling frictional cohesive powder are comparable to the effects of increasing ϕ towards ϕ_{RCP} in a tapped frictionless noncohesive powder. In other words, we assume that the "free void volume" vanishes for $\phi < \phi_{\mathrm{ALP}}$ because ϕ cannot be reduced any further without destabilizing the powder, and therefore the characteristic time for assembly processes that will produce settled packings with $\phi = \phi_{\mathrm{ALP}}$ is astronomical, but that this time *decreases* exponentially with increasing ϕ.

Assuming that $\tau_{\mathrm{slow}}^{-1}$ is the "attempt rate" for processes that form a mechanically stable settled sample, replacing the tapping-experiment duration t (Eq. 1) with the pouring-experiment duration τ_{ramp}, and adapting the procedure used in Section 2.1 of Ref. [29] to the above-mentioned assumptions about free void volume leads to the prediction

$$\exp\left[\frac{\phi_{\mathrm{settled}}(0) - \phi_{\mathrm{ALP}}}{\phi_{\mathrm{settled}}(\tau_{\mathrm{ramp}}) - \phi_{\mathrm{ALP}}}\right] = \exp(1)\left(1 + \frac{\tau_{\mathrm{ramp}}}{\tau_{\mathrm{slow}}}\right)^B, \tag{3}$$

where $\phi_{\mathrm{settled}}(0)$ is the packing fraction obtained in the fast-pouring limit where minimal aggregation and compact-cluster stabilization occurs prior to settling [55], and B is a free parameter that depends on factors such as the grains' size distribution and stiffness. Rearranging Eq. 3 leads to the rate law

$$\phi_{\mathrm{settled}}(\tau_{\mathrm{ramp}}) = \phi_{\mathrm{ALP}} + \frac{\phi_{\mathrm{settled}}(0) - \phi_{\mathrm{ALP}}}{1 + B\ln\left(1 + \tau_{\mathrm{ramp}}/\tau_{\mathrm{slow}}\right)}. \tag{4}$$

As illustrated in Fig. 1(c), Equation 4 accurately describes model 4's $\phi_{\mathrm{settled}}(\tau_{\mathrm{ramp}})$. Notably, it predicts that frictional cohesive powders have *ultraslow* settling kinetics in the sense that their ϕ_{settled} continues decreasing steadily with increasing τ_{ramp} even with τ_{ramp} is *very* large [56]. Comparably slow kinetics are predicted by some "parking lot" models of granular compaction – see e.g. Fig. 2 of Ref. [57] – but these models have not yet been adapted to capture the consequences of structural void stabilization.

Equation 4 should also predict the settling kinetics of real powders in the limit of strong intergrain cohesion and friction, e.g. Geldart Group C [58] powders with average grain size $\lesssim 10\mu m$, when the pouring height is small or the settling takes place in a gas-fluidized bed. A direct experimental test of its validity could potentially be performed by starting with a well-fluidized deagglomerated micropowder [17, 59], and then comparing the ϕ_{settled} obtained after imposing a variety of gas-flow histories $v_g(t) = v_g(0)[1 - t/\tau_{\mathrm{ramp}}]$, where $v_g(0)$ is above the critical fluidization velocity v_c [60] and the set of τ_{ramp} employed spans at least ~ 3 orders of magnitude. Performing such experiments and better understanding the ultraslow kinetics of frictional cohesive powder settling could ultimately help develop more-robust processing strategies for micropowders; developing such strate-

gies is a major current challenge in the pharmaceutical and additive-manufacturing industries [31, 32].

We thank Andrew Santos, Ishan Srivastava, Abhinen-

[1] J. B. Knight, C. G. Fandrich, C. N. Lau, H. M. Jaeger, and S. R. Nagel, "Density relaxation in a vibrated granular material," Phys. Rev. E **51**, 3957 (1995).

[2] P. Richard, M. Nicodemi, R. Delannay, P. Ribiére, and D. Bideau, "Slow relaxation and compaction of granular systems," Nat. Mat. **4**, 121 (2005).

[3] A. J. Kovacs, R. A. Stratton, and J. D. Ferry, "Dynamic mechanical properties of polyvinyl acetate in shear in the glass transition temperature range," J. Phys. Chem. **67**, 152 (1963).

[4] P. G. Debenedetti and F. H. Stillinger, "Supercooled liquids and the glass transition," Nature **410**, 259 (2001).

[5] A. J. Liu and S. R. Nagel, "The jamming transition and the marginally jammed solid," Ann. Rev. Cond. Matt. Phys. **1**, 347 (2010).

[6] L. Berthier and G. Tarjus, "Nonperturbative effect of attractive forces in viscous liquids," Phys. Rev. Lett. **103**, 170601 (2009).

[7] C. S. Campbell, "Rapid granular flows," Ann. Rev. Fluid Mech. **22**, 57 (1990).

[8] J. A. TenCate, E. Smith, and R. A. Guyer, "Universal slow dynamics in granular solids," Phys. Rev. Lett. **85**, 1020 (2000).

[9] D. Kadau, G. Bartels, L. Brendel, and D. E. Wolf, "Pore stabilization in cohesive granular systems," Phase Trans. **76**, 315 (2003).

[10] G. Bartels, T. Unger, D. Kadau, D. E. Wolf, and J. Kertesz, "The effect of contact torques on porosity of cohesive powders," Gran. Matt. **7**, 139 (2005).

[11] N. Vandewalle, G. Lumay, O. Gerasimov, and F. Ludeveig, "The influence of grain shape, friction and cohesion on granular compaction dynamics," Eur. Phys. J. E **22**, 241 (2007).

[12] F. A. Gilabert, J. N. Roux, and A. Castellanos, "Computer simulation of model cohesive powders: Influence of assembling procedure and contact laws on low consolidation states," Phys. Rev. E **75**, 011303 (2007).

[13] F. A. Gilabert, J. N. Roux, and A. Castellanos, "Computer simulation of model cohesive powders: Plastic consolidation, structural changes, and elasticity under isotropic loads," Phys. Rev. E **78**, 031305 (2008).

[14] D. Kadau, "From powders to collapsing soil/living quicksand: Discrete modeling and experiment," AIP Conf. Proc. **1227**, 50 (2010).

[15] H. H. Hausner, "Friction conditions in a mass of metal powder," Int. J. Powder Metallurg. **3**, 7 (1967).

[16] J. W. Carson and B. H. Pittenger, "Bulk properties of powders," in *ASME Handbook vol. 7: Powder metal technologies and applications*, edited by P. W. Lee, Y. Trudel, R. Iacocca, R. M. German, B. I. Ferguson, K. Moyer, D. Madan, and Sanderow H (ASM International, 1998) p. 287.

[17] J. Blum and R. Schräpler, "Structure and mechanical properties of high-porosity macroscopic agglomerates formed by random ballistic deposition," Phys. Rev. Lett. **93**, 115503 (2004).

[18] J. E. Fiscina, G. Lumay, F. Ludewig, and N. Vandewalle, "Compaction dynamics of wet granular assemblies," Phys. Rev. Lett. **105**, 048001 (2010).

[19] W. Liu, S. Li, A. Baule, and H. A. Makse, "Adhesive loose packings of small dry particles," Soft Matt. **11**, 6492 (2015).

[20] W. Liu, Y. Jin, S. Chen, H. A. Makse, and S. Li, "Equation of state for random sphere packings with arbitrary adhesion and friction," Soft Matt. **13**, 421 (2017).

[21] A. Santomaso, P. Lazzaro, and P. Canu, "Powder flowability and density ratios: the impact of granules packing," Chem. Eng. Sci. **58**, 2857 (2006).

[22] "Standard Test Method for Apparent Density of Free-Flowing Metal Powders Using the Hall Flowmeter Funnel", ASTM-B212, American Society for Testing and Materials.

[23] K. Traina, R. Cloots, S. Bontempi, G. Lumay, N. Vandewalla, and F. Boschini, "Flow abilities of powders and granular materials evidenced from dynamical tap density measurement," Powder Tech. **235**, 842 (2013).

[24] J. Schmidt, E. J. R. Parteli, N. Uhlmann, N. Wörlein, K.-E. Wirth, T. Pöschel, and W. Peuker, "Packings of micron-sized spherical particles: Insights from bulk density determination, X-ray microtomography and discrete element simulations," Adv. Powd. Tech. **31**, 2293 (2020).

[25] A. Lemaitre, C. Mondal, I. Procaccia, S. Roy, Y. Wang, and J. Zhang, "Frictional granular matter: Protocol dependence of mechanical properties," Phys. Rev. Lett. **126** (2021).

[26] T. Boutreux and P. G. de Gennes, "Compaction of granular mixtures: a free volume model," Physica A **244**, 59 (1997).

[27] E. Ben-Naim, J. B. Knight, E. R. Nowak, H. M. Jaeger, and S. R. Nagel, "Slow relaxation in granular compaction," Physica D **123**, 380 (1998).

[28] S. F. Edwards and D. V. Grinev, "Statistical mechanics of vibration-induced compaction of powders," Phys. Rev. E **58**, 4758 (1998).

[29] T. Hao, "Tap density equations of granular powders based on the rate process theory and the free volume concept," Soft Matt. **11**, 1554 (2015).

[30] T. Mede, G. Chambon, F. Nicot, and P. Hagenmuller, "Micromechanical investigation of snow failure under mixed-mode loading," Int. J. Sol. Struct. **199**, 95 (2020).

[31] H. P. Goh, P. W. S. Heng, and C. V. Liew, "Comparative evaluation of powder flow parameters with reference to t particle size and shape," Int. J. Pharmeceut. **547**, 133 (2018).

[32] S. Vock, B. Klöden, A. Kirchner, T. Weißgärber, and B. Kieback, "Powders for powder bed fusion: a review," Prog. Add. Manufact. **4**, 383 (2019).

[33] H. P. Zhang and H. A. Makse, "Jamming transition in emulsions and granular materials," Phys. Rev. E **72**, 011301 (2005).

[34] M. P. Ciamarra, A. Coniglio, and A. de Candia, "Disordered jammed packings of frictionless spheres," Soft

Matt. **6**, 2975 (2010).

[35] P. Chaudhuri, L. Berthier, and S. Sastry, "Jamming transitions in amorphous packings of frictionless spheres occur over a continuous range of volume fractions," Phys. Rev. Lett. **104**, 165701 (2010).

[36] P. G. Rognon, J.-N. Roux, D. Wolf, M. Naaïm, and F. Chevoir, "Rheophysics of cohesive granular materials," Europhys. Lett. **74**, 644 (2006).

[37] P. G. Rognon, J.-N. Roux, M. Naaïm, and F. Chevoir, "Dense flows of cohesive granular materials," J. Fluid. Mech, **596**, 21 (2008).

[38] N. V. Brilliantov, F. Spahn, J. M. Hertzch, and T. Poschel, "Model for collisions in granular gases," Phys. Rev. E **53**, 5382 (1996).

[39] L. E. Silbert, D. Ertas, G. S. Grest, T. C. Halsey, and D. Levine, "Granular flow down an inclined plane: Bagnold scaling and rheology," Phys. Rev. E **64**, 051302 (2001).

[40] A. P. Santos, D. S. Bolintineanu, G. S. Grest, J. B. Lechman, S. J. Plimpton, and I. Srivastava, "Granular packings with sliding, rolling, and twisting friction," Phys. Rev. E **102**, 032903 (2020).

[41] S. Luding, "Cohesive, frictional powders: contact models for tension," Gran. Matt. **10**, 235 (2008).

[42] G. D. Scott and D. M. Kilgour, "The density of random close packing of spheres," J. Phys. D Appl. Phys. **2**, 86 (1969).

[43] M. Jerkins, M. Schröter, H. L. Swinney, T. J. Senden, M. Saadatfar, and T. Aster, "Onset of mechanical stability in random packings of frictional spheres," Phys. Rev. Lett. **101**, 018301 (2008).

[44] G. R. Farrell, K. M. Martini, and N. Menon, "Loose packings of frictional spheres," Soft Matt. **6**, 2925 (2010).

[45] C. S. O'Hern, L. E. Silbert, A. J. Liu, and S. R. Nagel, "Jamming at zero temperature and zero applied stress: The epitome of disorder," Phys. Rev. E **68**, 011306 (2003).

[46] L. E. Silbert, "Jamming of frictional spheres and random loose packing," Soft Matt. **6**, 2918 (2010).

[47] A. P. Thompson *et al.*, "Lammps-a flexible simulation tool for particle-based materials modeling at the atomic, meso, and continuum scales," Comp. Phys. Comm. **271**, 108171 (2022).

[48] Note that these applied stresses are the *target* values imposed by the Nose-Hoover barostat employed in these simulations. Deviations of the actual $\bar{\sigma}$ from these target values, caused, e.g., by particle rearrangements, are damped with a damping time $\tau_{\text{damp}} = 500$. Thus our compression protocol allows for density fluctuations "on top of" the overall trends in $\phi(t)$. These can produce excitations that allow for further densification, analogous to those that occur during tapping experiments [1, 2].

[49] Throughout these simulations, the periodic-cell side lengths $L_x(t)$, $L_y(t)$ and $L_z(t)$ vary independently, so the final simulation cell is (in general) orthorhombic. Ref. [40] showed that the stability of marginally jammed states against shear is optimized by compression protocols that also maintain the three shear stresses σ_{xy}, σ_{xz}, and σ_{yz} at zero during compression and thus end up with triciinic simulation cells. We performed compression runs for all four models using such a protocol, and found that in all cases differences in the results discussed below were negligible.

[50] R. J. Speedy, "The hard sphere glass transition," Mol. Phys. **95**, 169 (1998).

[51] J. Hopcroft and R. Tarjan, "Algorithm 447: efficient algorithms for graph manipulation," Comm. ACM **16**, 372 (1973).

[52] G. Lois and C. S. O'Hern, "Jamming transition and new percolation universality classes in particulate systems with attraction," Phys. Rev. Lett. **100**, 028001 (2008).

[53] D. J. Koeze and B. P. Tighe, "Sticky matters: Jamming and rigid cluster statistics with attractive particle interactions," Phys. Rev. Lett. **121** (2018).

[54] D. J. Koeze, L. Hong, A. Kuman, and B. P. Tighe, Elasticity of jammed packings of sticky disks Phys. Rev. Res. **2**, 032047 (2020).

[55] M. Dong, Z. Wang, and Y. Gan, "Wet mono-sized granular packing: effects of initial clusters and filling strategy," Powd. Tech. **407**, 117678 (2022).

[56] For example, it predicts that model 4's ϕ_{settled} decreases from ~ 0.282 to ~ 0.245 (~ 0.223 to ~ 0.209) over the range $10^9 \leq \tau_{\text{ramp}} \leq 10^{12}$ ($10^{15} \leq \tau_{\text{ramp}} \leq 10^{18}$).

[57] P. Silbani and S. Boettcher, "Record dynamics in the parking-lot model," Phys. Rev. E **93**, 062141 (2016).

[58] D. Geldart, "Types of gas fluidization," Powd. Tech. **7**, 285 (1973).

[59] F. Raganati, R. Chirone, and P. Ammendola, "Gas–solid fluidization of cohesive powders," Chem. Eng. Res. Des. **133**, 347 (2018).

[60] J. M. Valverde, A. Castellanos, and M. A. S. Quintanilla, "Self-diffusion in a gas-fluidized bed of fine powder," Phys. Rev. Lett. **86**, 3020 (2001).